Variable-Number Variable-Band Selection for Feature Characterization in Hyperspectral Signatures

Su Wang, *Member, IEEE*, and Chein-I Chang, *Senior Member, IEEE*

***Abstract*—This paper presents a novel band selection-based feature characterization technique for a hyperspectral signature, which is referred to as variable-number variable-band selection (VNVBS). Since a hyperspectral signature can be uniquely characterized by its spectral profile, its feature characterization can be achieved by selecting appropriate bands from the original set of spectral bands, and the number of bands to be selected is totally determined by its original spectral shape. As a result, two hyperspectral signatures may require different sets of bands for spectral feature characterization. Therefore, the proposed VNVBS allows one to select a different number of variable bands in accordance with the hyperspectral signature to be processed. In order for the VNVBS to select an appropriate subset of bands for a hyperspectral signature, a new band prioritization criterion (BPC), which is referred to as orthogonal subspace projector based BPC, is derived. It assigns a different priority score to each spectral band of a hyperspectral signature such that various features can be captured by the VNVBS. Accordingly, the VNVBS can be interpreted as a spectral feature extraction technique for hyperspectral signature characterization. Finally, experiments using two data sets are conducted to demonstrate that the VNVBS can improve the performance of the hyperspectral signature characterization.**

***Index Terms*—Band prioritization (BP), hyperspectral-signature characterization, orthogonal subspace projection based BP criterion (OSP-BPC), variable-number variable-band selection (VNVBS).**

I. Introduction

HYPERSPECTRAL data are collected by hundreds of contiguous and highly correlated spectral bands. Consequently, the same spectral bands that are used to acquire two different hyperspectral signatures may not provide the same level of signature information. Furthermore, recent advances in sensor technology have made it possible for one single sensor data to be acquired by more than hundreds or thousands of spectral channels, e.g., ultraspectral data. Of particular interest is the chemical/biological (CB) defense for bioterrorism where the CB data available for analysis are generally spectral data rather than image data. However, it also comes at a price that such wealthy spectral information is highly correlated. Consequently, using all the hundreds or thousands of spectral channels might not be a good choice in preserving the spectral information since a significant and crucial piece of information of interest may be only provided by a very narrow range of spectral coverage which could be overwhelmed by other dominating spectral channels. For example, the crucial information of chemical data is provided by the thermal range, and the biological data are determined by their distinct protein spectral profiles which are usually very small and can be only captured by very narrow diagnostic spectral channels. Therefore, the information provided by their spectral profiles becomes vital, and the band selection (BS)-based spectral signature analysis and characterization seem to be the most effective means to address this issue.

BS has been widely used in remote sensing image analysis for various reasons [1]–[5]. To the authors' best knowledge, most of the existing BS techniques are developed for images where the number of bands is fixed and the bands selected for each image pixel are identical. Unfortunately, a direct application of such image-based BS to the single spectral signature analysis and characterization seems not to work due to the following two reasons. One is that no sample spectral information among pixels that has been used by image-based BS is also available for a hyperspectral signature. The other is that a different hyperspectral signature may require a different number of bands as well as different spectral bands to characterize its spectral profile. More specifically, in order to characterize a spectral signature effectively, a variable band number and variable bands should be used for the spectral signature analysis. This paper takes up this challenging task and presents a new concept, which is referred to as variable-number variable-band selection (VNVBS) with its main focus placed on a single hyperspectral signature rather than a hyperspectral image.

There are two major differences between our proposed VNVBS and the existing BS techniques. First, the BS techniques that are commonly used in remote sensing image processing are generally image-based approaches. The BS is developed by exploring the correlation among spectral images. By contrast, the VNVBS only deals with the single hyperspectral signatures which may come from a database or a spectral library, not an image. As a result, there is no correlation among image pixels that can be used by the VNVBS.

Manuscript received May 12, 2006; revised March 10, 2007.

S. Wang was with the Remote Sensing Signal and Image Processing Laboratory, Department of Computer Science and Electrical Engineering, University of Maryland Baltimore County, Baltimore, MD 21250 USA. She is now with the Health Science Center, Medical School, State University of New York at Stony Brook, Stony Brook, NY 11794 USA (e-mail: suwang@mil.sunysb.edu).

C.-I Chang is with the Remote Sensing Signal and Image Processing Laboratory, Department of Computer Science and Electrical Engineering, University of Maryland Baltimore County, Baltimore, MD 21250 USA, and also with the Environmental Restoration and Disaster Reduction Research Center and Department of Electrical Engineering, National Chung Hsing University, Taichung 402, Taiwan, R.O.C. (e-mail: cchang@umbc.edu).

Color of one or more of the figures in this paper are available online at http://ieeexplore.ieee.org.

Digital Object Identifier 10.1109/TGRS.2007.901051

Instead, the only available information that can be used by the VNVBS is the spectral band-to-band correlation within a single hyperspectral signature. Therefore, compared to the image-based BS which deals with a 3-D image cube, the VNVBS actually operates on 1-D hyperspectral signatures, and thus, it can be considered as 1-D signature-based BS. Second, the band numbers and the bands selected for each individual image-pixel vector by the conventional image-based BS are always fixed and identical. On the contrary, the VNVBS selects a variable band number and variable bands for each of the hyperspectral signatures to be processed. In doing so, two key issues must be addressed as follows: 1) "How many bands are required for the VNVBS to select for a hyperspectral signature?;" and 2) "what are these particularly selected bands?" Both of these issues can be simultaneously addressed by a new approach proposed in this paper, which is referred to as orthogonal-subspace-projector-based band prioritization criterion (OSP-BPC) along with the so-called reference signature. The OSP-BPC decomposes a hyperspectral signature $\mathbf{s}$ to be processed into two OSP components with respect to the reference signature from which a score for each particular band can be derived for prioritization. By virtue of the OSP-BPC, the original band set Ω of a hyperspectral signature can be rearranged and divided into two disjoint sets, which are denoted by $\Omega_{\mathbf{s}}^{\perp}$ and $\Omega_{\mathbf{s}}$, in accordance with the OSP-BPC assigned priority score for each band. Only those bands derived from $\Omega_{\mathbf{s}}^{\perp}$ have higher priorities than those in $\Omega_{\mathbf{s}}$. Since the bands from $\Omega_{\mathbf{s}}^{\perp}$ vary with the hyperspectral signature $\mathbf{s}$ to be processed, two different hyperspectral signatures may result in different sets of $\Omega_{\mathbf{s}}^{\perp}$ because of the following: 1) the number of bands to be selected is different; and 2) the selected bands are also different.

One interesting finding is noteworthy. The VNVBS can be used as a feature selection method. Compared to other traditional spectral similarity measures such as Euclidean distance (ED), Spectral Angle Mapper (SAM) [6], [7], and also spectral information divergence (SID) [6], [7] which utilizes all the full-band information, the VNVBS judiciously selects bands that can best describe the spectral characterization in the sense of OSP. As a consequence, it can remove redundant spectral information while retaining vital and crucial information to improve the performance in spectral signature analysis and characterization.

The remainder of this paper is organized as follows. Section II derives an OSP-BPC, and Section III presents a new technique, VNVBS is developed. Section IV conducts experiments for the VNVBS in applications of hyperspectral-signature characterization, such as classification, identification, and discrimination. Section V provides some general guidelines on the selection of reference signature, and Section VI concludes some remarks.

II. Orthogonal Subspace Projection-Based Band Prioritization Criterion

The OSP approach has been widely used for hyperspectral target detection and classification [8]. It extends a standard signal-detection model by dividing the signatures of interest into two types, called desired target signature $\mathbf{d}$, which is to be detected, and undesired target signatures, which are to be eliminated. The performance in detecting $\mathbf{d}$ can be improved by eliminating the undesired signatures prior to the detection of $\mathbf{d}$. This section extends the OSP concept to a BPC.

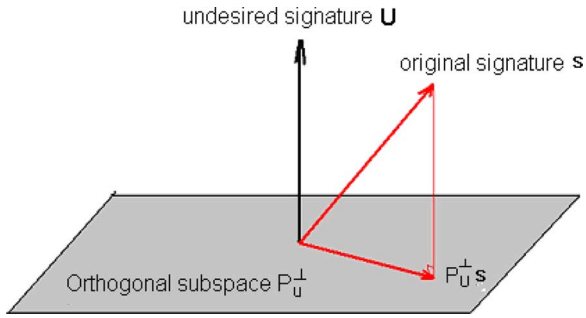

Fig. 1. Geometric interpretation of OSP.

Assume that $\mathbf{U}$ is the undesired signature matrix formed by placing all the undesired target signatures as its column vectors. In order to eliminate all signatures in the $\mathbf{U}$, a projector developed in [8] can be used for this purpose, which is given by

$$P_{\mathbf{U}}^{\perp} = \mathbf{I} - \mathbf{U}\mathbf{U}^{\#} \tag{1}$$

where $\mathbf{U}^{\#} = (\mathbf{U}^{\mathrm{T}}\mathbf{U})^{-1}\mathbf{U}^{\mathrm{T}}$ is the pseudo-inverse of $\mathbf{U}$, and $\mathbf{I}$ is an identity matrix. Applying $P_{\mathbf{U}}^{\perp}$ to a hyperspectral signature $\mathbf{s}$ leads to a new signature denoted by $\hat{\mathbf{s}}$ defined as follows:

$$\hat{\mathbf{s}} = P_{\mathbf{U}}^{\perp}\mathbf{s} = (\mathbf{I} - \mathbf{U}\mathbf{U}^{\#})\mathbf{s} \tag{2}$$

where the undesired signatures in $\mathbf{U}$ have been eliminated from the original signature $\mathbf{s}$, and $\mathbf{s}$ has been projected onto the subspace $P_{\mathbf{U}}^{\perp}$, becoming $\hat{\mathbf{s}}$. The geometric relationship between $\mathbf{s}$, $P_{\mathbf{U}}^{\perp}$ and $\hat{\mathbf{s}}$ can be interpreted in Fig. 1.

By taking advantage of the concept of OSP outlined by (1) and (2), a hyperspectral signature can be decomposed into two orthogonal projection components. After this OSP, the spectral bands of a hyperspectral signature can be ranked and selected according to their priorities measured by an OSP-based criterion, referred to as OSP-BPC, which is presented in detail as follows.

Assume that $\mathbf{s} = (s_1, s_2, \ldots s_L)^{\mathrm{T}}$ is a hyperspectral signature to be processed and $\mathbf{r} = (r_1, r_2, \ldots r_L)^{\mathrm{T}}$ is the so-called reference signature against which the $\mathbf{s}$ is compared, where L denotes the total number of bands used to acquire the signature $\mathbf{s}$. Two orthogonal projectors based on the reference signature $\mathbf{r}$, $P_{\mathbf{r}}$ and $P_{\mathbf{r}}^{\perp}$ can be further defined as follows [8]:

$$P_{\mathbf{r}} = \mathbf{r}\mathbf{r}^{\#} \tag{3}$$

$$P_{\mathbf{r}}^{\perp} = \mathbf{I} - P_{\mathbf{r}} \tag{4}$$

where $\mathbf{r}^{\#} = (\mathbf{r}^{\mathrm{T}}\mathbf{r})^{-1}\mathbf{r}^{\mathrm{T}}$ is the pseudo-inverse of $\mathbf{r}$. By means of (3) and (4), the hyperspectral signature $\mathbf{s}$ can be projected onto two orthogonal subspaces $P_{\mathbf{r}}^{\perp}$ and $P_{\mathbf{r}}$ and decomposed into two orthogonal projection components $\mathbf{s}_{\mathbf{r}}^{\perp}$ and $\mathbf{s}_{\mathbf{r}}$, which are defined by

$$\begin{aligned} \mathbf{s}_{\mathbf{r}}^{\perp} &= P_{\mathbf{r}}^{\perp}\mathbf{s} = (\mathbf{I} - \mathbf{r}\mathbf{r}^{\#})\mathbf{s} \\ \mathbf{s}_{\mathbf{r}} &= P_{\mathbf{r}}\mathbf{s} = (\mathbf{r}\mathbf{r}^{\#})\mathbf{s}. \end{aligned} \tag{5}$$

In general, the reference signature $\mathbf{r}$ is selected in such a way that it shares some information with the signature $\mathbf{s}$ to be processed so that $\mathbf{s}_{\mathbf{r}}^{\perp}$ will be nonempty when $\mathbf{s}$ is projected onto $P_{\mathbf{r}}^{\perp}$ and $P_{\mathbf{r}}$ via (5). However, it should be noted that, on some occasions, the selected reference signature $\mathbf{r}$ may turn out to be either parallel to the signature $\mathbf{s}$ which results in $\mathbf{s}_{\mathbf{r}}^{\perp} = \varnothing$ or orthogonal to the signature $\mathbf{s}$ which results in $\mathbf{s}_{\mathbf{r}} = \varnothing$.

Accordingly, a new OSP-based criterion referred to as OSP-BPC can be derived as follows.

A. OSP-BPC Algorithm

1) Pre-process the signature $\mathbf{s}$ by expanding the $\mathbf{s}$ into $(L+4)$-dimensional column vector by adding two zeros to both the head and the tail of $\mathbf{s}$ into the form of $(0, 0, s_1, s_2, \ldots, s_L, 0, 0)$.
2) Assume that the spectral value on the lth band of the signature $\mathbf{s}$ is s_l, $l = 1, 2, \ldots, L$. Group its four neighboring bands s_{l-2}, s_{l-1}, s_{l+1}, and s_{l+2} from [0, 0, $\mathbf{s}$, 0, 0] to form a vector centered at s_l which is defined by

$$\mathbf{s}_l^5 = (s_{l-2}, s_{l-1}, s_l, s_{l+1}, s_{l+2})^{\mathrm{T}}. \tag{6}$$

Similarly, for the l-band of two orthogonal components $\mathbf{s}_{\mathbf{r}}^{\perp}$ and $\mathbf{s}_{\mathbf{r}}$, which are denoted by $\mathbf{s}_{\mathbf{r}_l}^{\perp}$ and $\mathbf{s}_{\mathbf{r}_l}$, we can also define $(\mathbf{s}_{\mathbf{r}}^{\perp})_l^5$ and $(\mathbf{s}_{\mathbf{r}})_l^5$ as follows:

$$\begin{aligned}\left(\mathbf{s}_{\mathbf{r}}^{\perp}\right)_l^5 &= \left(s_{\mathbf{r}_{l-2}}^{\perp}, s_{\mathbf{r}_{l-1}}^{\perp}, s_{\mathbf{r}_l}^{\perp}, s_{\mathbf{r}_{l+1}}^{\perp}, s_{\mathbf{r}_{l+2}}^{\perp}\right)^{\mathrm{T}} \\ (\mathbf{s}_{\mathbf{r}})_l^5 &= \left(s_{\mathbf{r}_{l-2}}, s_{\mathbf{r}_{l-1}}, s_{\mathbf{r}_l}, s_{\mathbf{r}_{l+1}}, s_{\mathbf{r}_{l+2}}\right)^{\mathrm{T}}.\end{aligned} \tag{7}$$

3) Calculate the inner products between the vector $\mathbf{s}_l^5$ and the two vectors $(\mathbf{s}_{\mathbf{r}}^{\perp})_l^5$ and $(\mathbf{s}_{\mathbf{r}})_l^5$ defined in (7) by

$$\begin{aligned}\left\langle \mathbf{s}_l^5, \left(\mathbf{s}_{\mathbf{r}}^{\perp}\right)_l^5 \right\rangle &= \left(\mathbf{s}_l^5\right)^{\mathrm{T}} \left(\mathbf{s}_{\mathbf{r}}^{\perp}\right)_l^5 \\ \left\langle \mathbf{s}_l^5, (\mathbf{s}_{\mathbf{r}})_l^5 \right\rangle &= \left(\mathbf{s}_l^5\right)^{T} (\mathbf{s}_{\mathbf{r}})_l^5.\end{aligned} \tag{8}$$

4) For the lth band s_l, there is a pair of priority scores associated with it, which is defined by

$$\left(\left\langle \mathbf{s}_l^5, \left(\mathbf{s}_{\mathbf{r}}^{\perp}\right)_l^5 \right\rangle, \left\langle \mathbf{s}_l^5, (\mathbf{s}_{\mathbf{r}})_l^5 \right\rangle\right). \tag{9}$$

5) Based on (9), the original band set $\Omega = \{1, 2, \ldots, L\}$ can be divided into two disjoint subsets, denoted by $\Omega_{\mathbf{s}}^{\perp}$ and $\Omega_{\mathbf{s}}$, which are defined by

$$\begin{aligned}\Omega_{\mathbf{s}}^{\perp} &= \left\{ l : \left\langle \mathbf{s}_l^5, \left(\mathbf{s}_{\mathbf{r}}^{\perp}\right)_l^5 \right\rangle > \left\langle \mathbf{s}_l^5, (\mathbf{s}_{\mathbf{r}})_l^5 \right\rangle, \qquad l = 1, 2, \ldots L \right\} \\ \Omega_{\mathbf{s}} &= \left\{ l : \left\langle \mathbf{s}_l^5, \left(\mathbf{s}_{\mathbf{r}}^{\perp}\right)_l^5 \right\rangle < \left\langle \mathbf{s}_l^5, (\mathbf{s}_{\mathbf{r}})_l^5 \right\rangle, \qquad l = 1, 2, \ldots L \right\}\end{aligned} \tag{10}$$

such that $\Omega_{\mathbf{s}}^{\perp}$ collects those bands that contain more information in $P_{\mathbf{r}}^{\perp}$ than in $P_{\mathbf{r}}$ in the sense of orthogonal projection, while the set $\Omega_{\mathbf{s}}$ does oppositely.

The motivation of using four adjacent neighboring bands in (6) comes from the image processing which uses four- and eight-neighbor connectivities to account for interpixel spatial correlation within a 3×3 window [9]. This idea is extended to the spectral domain to capture the interband correlation within a five-band 1×5 window. Of course, the same idea can also be applied to seven-band, nine-band windows, etc. However, based on our experiments, using the five-band 1×5 window seems to be the best compromise because using a window of a band number greater than five has little improvement on the performance at the expense of computational complexity, while using the five-band window, indeed, improves significantly over using the three-band window.

III. Variable-Number Variable-Band Selection

The pair of $\langle \mathbf{s}_l^5, (\mathbf{s}_{\mathbf{r}}^{\perp})_l^5 \rangle$ and $\langle \mathbf{s}_l^5, (\mathbf{s}_{\mathbf{r}})_l^5 \rangle$ defined in (8), associated with the lth band s_l, is considered as the two correlated prioritization scores of the lth band, which are essentially two pieces of information contained in the two orthogonal subspaces $P_{\mathbf{r}}^{\perp}$ and $P_{\mathbf{r}}$. Due to the principle of orthogonality [10], the information in $P_{\mathbf{r}}^{\perp}$ generally provides innovative information about the signature $\mathbf{s}$ with respect to the reference signature $\mathbf{r}$. Therefore, only the $\langle \mathbf{s}_l^5, (\mathbf{s}_{\mathbf{r}}^{\perp})_l^5 \rangle$ in (8) is used to rank the bands in Ω according to the decreasing order of its magnitude. The resulting $\langle \mathbf{s}_l^5, (\mathbf{s}_{\mathbf{r}}^{\perp})_l^5 \rangle$-priority-ranked band set can be further broken up into two disjoint sets $\Omega_{\mathbf{s}}^{\perp}$ and $\Omega_{\mathbf{s}}$, which are determined by (10). By realigning $\Omega_{\mathbf{s}}^{\perp}$ and $\Omega_{\mathbf{s}}$, a new priority-ranked band set will be generated for further BS, which is denoted by $\Omega_{\mathbf{s}}^{*}$

$$\Omega_{\mathbf{s}}^{*} = \left(\Omega_{\mathbf{s}}^{\perp}, \Omega_{\mathbf{s}}\right). \tag{11}$$

In what follows, the VNVBS is developed by only selecting those bands coming from the set $\Omega_{\mathbf{s}}^{\perp}$, based on the pair of priority scores defined by (9). Since the size of the set $\Omega_{\mathbf{s}}^{\perp}$ varies with the signature $\mathbf{s}$ to be prioritized, the number of bands to be selected for various hyperspectral signatures is not fixed *a priori* but rather determined by the comparison between $\langle \mathbf{s}_l^5, (\mathbf{s}_{\mathbf{r}}^{\perp})_l^5 \rangle$ and $\langle \mathbf{s}_l^5, (\mathbf{s}_{\mathbf{r}})_l^5 \rangle$ via (10).

In the hyperspectral-signature characterization, a frequently encountered application is signature discrimination, which involves two different signatures, which are denoted by $\mathbf{s}_1$ and $\mathbf{s}_2$, respectively. In this case, the VNVBS is implemented through the following steps, referred to as VNVBS-based hyperspectral signature discrimination (VNVBS-HSD).

A. VNVBS-Based Hyperspectral Signature Discrimination

1) Given two signatures to be discriminated $\mathbf{s}_1$ and $\mathbf{s}_2$, select a reference signature $\mathbf{r}$ on which both $\mathbf{s}_1$ and $\mathbf{s}_2$ are orthogonally projected. The issue of how to select the $\mathbf{r}$ will be discussed in detail at the end of Section IV.
2) Obtain the priority-ranked band sets produced by the $\mathbf{s}_1$ and $\mathbf{s}_2$, respectively, based on (3)–(10), with the results denoted by $\Omega_{\mathbf{s}_1}^{*} = (\Omega_{\mathbf{s}_1}^{\perp}, \Omega_{\mathbf{s}_1})$ and $\Omega_{\mathbf{s}_2}^{*} = (\Omega_{\mathbf{s}_2}^{\perp}, \Omega_{\mathbf{s}_2})$, respectively. A geometric interpretation of the relationship between $\Omega_{\mathbf{s}_1}^{*} = (\Omega_{\mathbf{s}_1}^{\perp}, \Omega_{\mathbf{s}_1})$ and $\Omega_{\mathbf{s}_2}^{*} = (\Omega_{\mathbf{s}_2}^{\perp}, \Omega_{\mathbf{s}_2})$ is shown in Fig. 2.

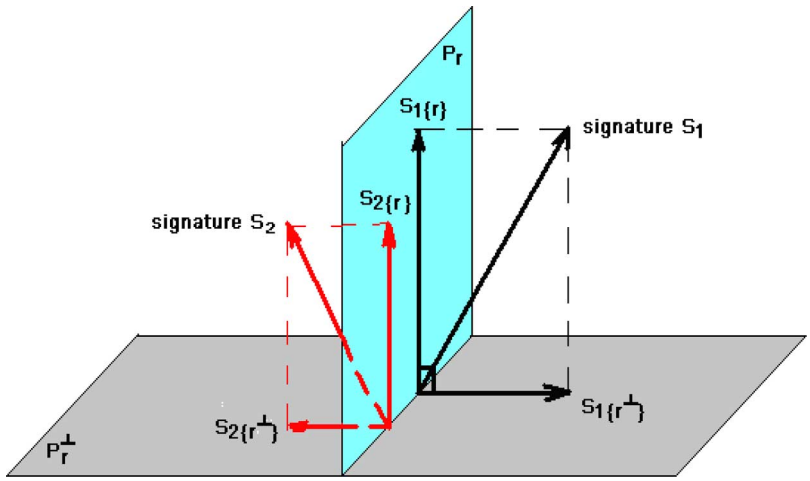

Fig. 2. Geometric interpretation of the relationship between $\Omega^*_{\mathbf{s}_1} = (\Omega^{\perp}_{\mathbf{s}_1}, \Omega_{\mathbf{s}_1})$ and $\Omega^*_{\mathbf{s}_2} = (\Omega^{\perp}_{\mathbf{s}_2}, \Omega_{\mathbf{s}_2})$.

3) Find a new band set, denoted by $\Omega^{\perp}(\mathbf{s}_1, \mathbf{s}_2)$, which is generated by $\Omega^{\perp}_{\mathbf{s}_1}$ and $\Omega^{\perp}_{\mathbf{s}_2}$ as follows:

$$\Omega^{\perp}(\mathbf{s}_1, \mathbf{s}_2) = \begin{cases} \Omega^{\perp}_{\mathbf{s}_1} \cap \Omega^{\perp}_{\mathbf{s}_2} & \text{if } \Omega^{\perp}_{\mathbf{s}_1} \cap \Omega^{\perp}_{\mathbf{s}_2} \neq \varnothing \\ \Omega^{\perp}_{\mathbf{s}_1} \cup \Omega^{\perp}_{\mathbf{s}_2} & \text{if } \Omega^{\perp}_{\mathbf{s}_1} \cap \Omega^{\perp}_{\mathbf{s}_2} = \varnothing. \end{cases} \tag{12}$$

In other words, $\Omega^{\perp}(\mathbf{s}_1, \mathbf{s}_2)$ is considered as those bands used for discrimination between the signatures $\mathbf{s}_1$ and $\mathbf{s}_2$ so that $\Omega^{\perp}(\mathbf{s}_1, \mathbf{s}_2)$ can best preserve the information required by $\mathbf{s}_1$ and $\mathbf{s}_2$ for the signature discrimination.

4) Generate two new signatures $\mathbf{s}^*_1$ and $\mathbf{s}^*_2$ for both signatures $\mathbf{s}_1$ and $\mathbf{s}_2$ based on the bands selected by (12).
5) Use a spectral similarity measure such as spectral angle SAM, SID, or ED to perform the signature discrimination on the signatures $\mathbf{s}^*_1$ and $\mathbf{s}^*_2$ obtained in step 4).

A note on the criterion specified by (12) is worthwhile.

1) For the case of nonempty intersection, i.e., $\Omega^{\perp}_{\mathbf{s}_1} \cap \Omega^{\perp}_{\mathbf{s}_2} \neq \varnothing$, $\Omega^{\perp}_{\mathbf{s}_1} \cap \Omega^{\perp}_{\mathbf{s}_2}$ is chosen due to the fact that it carries more critical spectral information than $\Omega^{\perp}_{\mathbf{s}_1} \cup \Omega^{\perp}_{\mathbf{s}_2}$ in discrimination between $\mathbf{s}_1$ and $\mathbf{s}_2$ based on the following two reasons.
   a) Since $\Omega^{\perp}_{\mathbf{s}_1}$ and $\Omega^{\perp}_{\mathbf{s}_2}$ retain more crucial local spectral information of $\mathbf{s}_1$ and $\mathbf{s}_2$ in $P^{\perp}_{\mathbf{r}}$ than that in $P_{\mathbf{r}}$ in terms of discriminating spectral signatures $\mathbf{s}_1$ and $\mathbf{s}_2$ via orthogonal projection, the bands in $\Omega^{\perp}_{\mathbf{s}_1} \cap \Omega^{\perp}_{\mathbf{s}_2}$ are the smallest band set that can achieve the best possible spectral discrimination between $\mathbf{s}_1$ and $\mathbf{s}_2$.
   b) On the other hand, if $\Omega^{\perp}_{\mathbf{s}_1} \cup \Omega^{\perp}_{\mathbf{s}_2}$ is chosen instead of $\Omega^{\perp}_{\mathbf{s}_1} \cap \Omega^{\perp}_{\mathbf{s}_2}$, the bands in $([\Omega^{\perp}_{\mathbf{s}_1} \cup \Omega^{\perp}_{\mathbf{s}_2}] - [\Omega^{\perp}_{\mathbf{s}_1} \cap \Omega^{\perp}_{\mathbf{s}_2}])$ may potentially reduce the discrimination power between $\mathbf{s}_1$ and $\mathbf{s}_2$ due to the fact that the bands in $\Omega^{\perp}_{\mathbf{s}_1} - (\Omega^{\perp}_{\mathbf{s}_1} \cap \Omega^{\perp}_{\mathbf{s}_2})$ and $\Omega^{\perp}_{\mathbf{s}_2} - (\Omega^{\perp}_{\mathbf{s}_1} \cap \Omega^{\perp}_{\mathbf{s}_2})$ are spectrally representative for either $\mathbf{s}_1$ or $\mathbf{s}_2$, but not for both. For example, using the bands from $\Omega^{\perp}_{\mathbf{s}_1} - (\Omega^{\perp}_{\mathbf{s}_1} \cap \Omega^{\perp}_{\mathbf{s}_2})$ may be effective in better differentiating $\mathbf{s}_1$ from $\mathbf{s}_2$, but not necessarily the other way around because the bands in $\Omega^{\perp}_{\mathbf{s}_1} - (\Omega^{\perp}_{\mathbf{s}_1} \cap \Omega^{\perp}_{\mathbf{s}_2})$ are not part of $\Omega^{\perp}_{\mathbf{s}_2}$ and cannot effectively discriminate $\mathbf{s}_2$ from $\mathbf{s}_1$ as those bands in $\Omega^{\perp}_{\mathbf{s}_2}$ do. Similarly, it is also true for the bands in $\Omega^{\perp}_{\mathbf{s}_2} - (\Omega^{\perp}_{\mathbf{s}_1} \cap \Omega^{\perp}_{\mathbf{s}_2})$ which have better discrimination of $\mathbf{s}_2$ from $\mathbf{s}_1$, but do not necessarily have better discrimination of $\mathbf{s}_1$ from $\mathbf{s}_2$. Therefore, if bands in both band sets $\Omega^{\perp}_{\mathbf{s}_1} - (\Omega^{\perp}_{\mathbf{s}_1} \cap \Omega^{\perp}_{\mathbf{s}_2})$ and $\Omega^{\perp}_{\mathbf{s}_2} - (\Omega^{\perp}_{\mathbf{s}_1} \cap \Omega^{\perp}_{\mathbf{s}_2})$ are selected, these bands may be able to discriminate one from another but may be also very likely to deteriorate the discrimination between $\mathbf{s}_2$ and $\mathbf{s}_1$. In other words, an improvement upon the discrimination of $\mathbf{s}_1$ from $\mathbf{s}_2$ using the bands from $\Omega^{\perp}_{\mathbf{s}_1} - (\Omega^{\perp}_{\mathbf{s}_1} \cap \Omega^{\perp}_{\mathbf{s}_2})$ may impair the discrimination of $\mathbf{s}_2$ from $\mathbf{s}_1$ and vice versa. We have conducted a comprehensive study on comparison between using $\Omega^{\perp}_{\mathbf{s}_1} \cup \Omega^{\perp}_{\mathbf{s}_2}$ and $\Omega^{\perp}_{\mathbf{s}_1} \cap \Omega^{\perp}_{\mathbf{s}_2}$ which demonstrated that selecting bands from $\Omega^{\perp}_{\mathbf{s}_1} \cap \Omega^{\perp}_{\mathbf{s}_2}$ outperformed those selected from $\Omega^{\perp}_{\mathbf{s}_1} \cup \Omega^{\perp}_{\mathbf{s}_2}$ in discrimination between $\mathbf{s}_1$ and $\mathbf{s}_2$ in both ways, i.e., discrimination of $\mathbf{s}_1$ from $\mathbf{s}_2$ as well as the discrimination of $\mathbf{s}_2$ from $\mathbf{s}_1$.
2) For the empty-intersection case, i.e., $\Omega^{\perp}_{\mathbf{s}_1} \cap \Omega^{\perp}_{\mathbf{s}_2}$, since no bands are in common, the best way to achieve both discrimination of $\mathbf{s}_1$ from $\mathbf{s}_2$ and discrimination of $\mathbf{s}_2$ from $\mathbf{s}_1$ is to select all the bands in $\Omega^{\perp}_{\mathbf{s}_1} \cup \Omega^{\perp}_{\mathbf{s}_2}$ for $\Omega^{\perp}(\mathbf{s}_1, \mathbf{s}_2)$, which turns out to be the smallest band set in discrimination between $\mathbf{s}_1$ and $\mathbf{s}_2$.

In order to have a better discrimination between $\mathbf{s}_1$ and $\mathbf{s}_2$, it must achieve both better discrimination of $\mathbf{s}_2$ from $\mathbf{s}_1$ and better discrimination of $\mathbf{s}_2$ from $\mathbf{s}_1$. Taking the intersection $\Omega^{\perp}_{\mathbf{s}_1} \cap \Omega^{\perp}_{\mathbf{s}_2}$ is the only way to accomplish our task while retaining the smallest possible band set.

Another note is also worth being mentioned. Despite the fact that the VNVBS-HSD is developed to discriminate one signature from another, its functionality is certainly not limited to the signature discrimination. For example, if a signature is known to be detected, the VNVBS-HSD turns out to be a detector for that particular signature. On the other hand, if a group of signatures of interest is available for classification, then the VNVBS can be used as a signature classifier. Furthermore, if there is a database to be used for signature identification, then the VNVBS can become a signature identifier.

Finally, we summarize the differences of the proposed VNVBS from the commonly used image-based BS techniques

[1]–[4] which are generally performed via various criteria such as variance, signal-to-noise ratio (SNR), and information divergence.

1) The VNVBS only involves the spectral correlation among individual bands within a hyperspectral signature as opposed to the conventional image-based BS techniques [1]–[4], which consider each individual band image as a whole. Therefore, the VNVBS must rely only on the interband spectral correlation to select bands comparing to the conventional image-based BS techniques which make use of the spectra correlation among image pixels to select bands. As a result, the number of bands to be selected by the VNVBS varies with the signature to be processed, while the number of bands chosen by the conventional image-based BS techniques is fixed for all image pixels.
2) The BPC used in the VNVBS is OSP-BPC, which is easy and simple to implement. It also deviates from the commonly used BS criteria such as variance, SNR, and information divergence [1]–[4].
3) The VNVBS can be performed on the hyperspectral signatures with different numbers of bands. In doing so, two approaches are suggested and demonstrated in Section IV-B3 for the CB data whose band numbers are different. One is to take their common bands to yield the same number of bands. The other is to take all bands together while performing zero interpolation if the bands in one signature are missing in the other signature. As a result, the two hyperspectral signatures acquired by different numbers of spectral bands can be prioritized by the OSP-BPC and characterized by the VNVBS in terms of their spectral features. Although these two strategies can also be applied to any spectral similarity measure, there is no follow-up prioritization for further spectral feature characterization as what the OSP-BPC does. This benefit cannot be gained by any band-selection technique developed for images.

IV. Experiments

In order to demonstrate the utility of the proposed VNVBS in hyperspectral signature characterization, two completely different data sets were used for experiments, and two particular applications, which are signature discrimination and signature classification/identification, were of interest and further considered for comparative analysis with the SAM and the SID that are used as spectral similarity measures. Nevertheless, other applications can also be explored for the VNVBS. Due to the limited space, they are not included in this paper.

A. Hyperspectral Data

The first data set is coming from the five Airborne Visible InfraRed Imaging Spectrometer (AVIRIS) reflectances, which are blackbrush, creosote leaves, dry grass, red soil, and sagebrush with their spectra shown in Fig. 3.

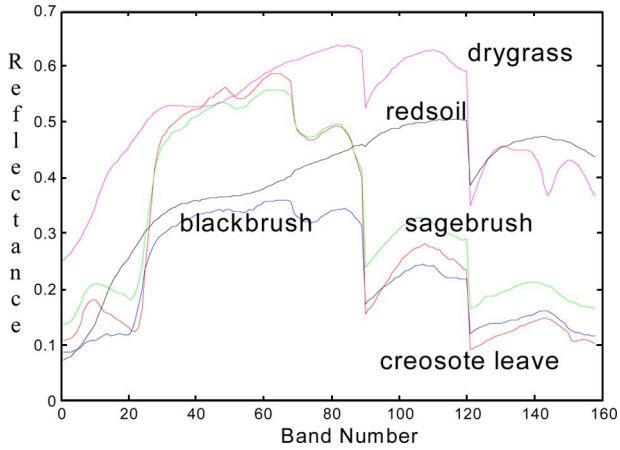

Fig. 3. Reflectances of creosote leaves, blackbrush, sagebrush, drygrass, and red soil.

TABLE I
$\Omega_{\mathbf{s}}^{\perp}$ AND $\Omega_{\mathbf{s}}$ FOR BLACKBRUSH, CREOSOTE LEAVES, AND SAGEBRUSH

$\mathbf{s}$	$\Omega_{\mathbf{s}}^{\perp}$	$\Omega_{\mathbf{s}}$
blackbrush	21-25, 91-98, 118-158	1-20, 26-90, 99-117
creosote leaves	empty	1-158
sagebrush	1-23, 92-100, 121-158	24-91, 101-120

Each of these five spectral signatures has 158 bands after water bands were removed and can be considered as a 158-D hyperspectral signature where each signature component is specified by a particular spectral wavelength. Based on Fig. 3, the spectral profiles of blackbrush, creosote leaves, and sagebrush are close among each other. In particular, the creosote leaves and sagebrush even have very close spectral values. A detailed quantitative analysis among these three signatures can be found in [5]. In this section, these five signatures constitute a spectral library or database to be used to evaluate the performance of the VNVBS in two different applications, which are the signature discrimination the classification/identification.

1) Signature Discrimination: In this case, three similar signatures, blackbrush, creosote leaves, and sagebrush, were used for discrimination, and the reference $\mathbf{r}$, as specified by (3) and (4), was chosen to be a signature obtained by averaging these three signatures $(\text{blackbrush} + \text{creosote leaves} + \text{sagebrush})/3$. Table I lists the bands that are prioritized by the VNVBS based on (9), where the original set of bands was divided into two subsets of bands $\Omega_{\mathbf{s}}^{\perp}$ and $\Omega_{\mathbf{s}}$ via (10).

As noted in Table I, the $\Omega_{\mathbf{s}}^{\perp}$ obtained for creosote leaves from the VNVBS via orthogonal-subspace decomposition was empty. This case occurred when either $\langle \mathbf{s}_l^5, (\mathbf{s}_{\mathbf{r}}^{\perp})_l^5 \rangle > \langle \mathbf{s}_l^5, (\mathbf{s}_{\mathbf{r}})_l^5 \rangle$ for all $l \in \{1, 2, \ldots, L\}$ or $\langle \mathbf{s}_l^5, (\mathbf{s}_{\mathbf{r}}^{\perp})_l^5 \rangle < \langle \mathbf{s}_l^5, (\mathbf{s}_{\mathbf{r}})_l^5 \rangle$ for all $l \in \{1, 2, \ldots, L\}$. However, it should be noted that whether or not a particular band is removed or preserved is completely determined by how a reference signature is selected and how the local spectral correlation described by (10) is involved among its four neighboring bands.

It is interesting to note that the VNVBS groups four band neighbors of a spectral band to generate a five-band vector

TABLE II
DISCRIMINATION AMONG BLACKBRUSH, CREOSOTE LEAVES, AND SAGEBRUSH USING (12) AND TABLE I

VNVBS \ full bands	(blackbrush, creosote)	(blackbrush, sagebrush)	(creosote, sagebrush)
SAM	0.1234 / 0.1767	0.0317 / 0.0681	0.1145 / 0.1289
SID	0.0161 / 0.0497	0.0011 / 0.0063	0.0140 / 0.0303

TABLE III
RESCALED DISCRIMINATION AMONG BLACKBRUSH, CREOSOTE LEAVES, AND SAGEBRUSH USING TABLE II

VNVBS \ full bands	(blackbrush, creosote)	(blackbrush, sagebrush)	(creosote, sagebrush)
SAM	3.89 / 2.59	1 / 1	3.61 / 1.89
SID	14.64 / 7.89	1 / 1	12.73 / 4.81

to capture its local spectral shape features rather than the spectral global tendency of a hyperspectral signature across the entire wavelengths. If we carefully compare the flat regions and edges of blackbrush, creosote leave, and sagebrush, the local spectral shapes captured by flat wavelengths of these three signatures are very close to each other, while the edges are much more different from each other. This finding explains why the VNVBS favored local edges rather than global flat regions. According to the OSP-BPC criterion, the global flat regions seem to contain redundant information which has no benefit to discrimination compared to the local edges which contain spectral characteristics that generally improve distance among the three signatures in terms of spectral similarity.

Table II tabulates the values of the SAM and the SID applied to the three VNVBS-generated new signatures of blackbrush, creosote leaves, and sagebrush by (12), where the upper and lower values were obtained by the original full band set and VNVBS, respectively, and the least discrimination results are shaded.

It is worth noting that the discriminatory power of a spectral measure is not determined by the magnitude of its spectral-similarity value but rather by the relative magnitude of one spectral value to another value. Therefore, even though the values of SAM and SID obtained by full bands were slightly larger than those obtained by the VNVBS, the ratio of one SAM (or SID) value to another SAM (or SID) value using the VNVBS was greatly increased compared to that using the full bands. In order to see this more clearly, we normalize the least discrimination results, which are the SAM or the SID values between blackbrush and sagebrush, to 1, then a new table can be generated in Table III from Table II, where it clearly shows that the relative discrimination between the two signatures was greatly improved by the VNVBS.

The aforementioned simple experiment demonstrated that the relative discrimination between these three signatures can be significantly increased if the VNVBS was used. This insight provides evidence that, in order to measure the effectiveness of the VNVBS relative to full bands, a direct comparison using Table II may not be appropriate. To address this issue, a measure suggested in [6] and [7], which is called the relative spectral discriminatory power (RSDPW), seems to fit our need and can be used for performance evaluation.

TABLE IV
RSDPW OF SAM AND SID WITH AND WITHOUT VNVBS

VNVBS \ full bands	(blackbrush, creosote)	(blackbrush, sagebrush)	(creosote, sagebrush)
SAM	2.3422 / 1.0715	1.3615 / 2.1693	3.1890 / 2.3244
SID	10.2230 / 1.5793	2.0333 / 3.7215	20.7859 / 5.8772

Assume that m is any given hyperspectral measure and $\mathbf{s}_1$, $\mathbf{s}_2$ are a pair of two spectral signatures to be measured. Let β be a third arbitrary signature with respect to which the two signatures $\mathbf{s}_1$, $\mathbf{s}_2$ are compared against. The RSDPW of m, which is denoted by $\text{RSDPW}_m(\mathbf{s}_1, \mathbf{s}_2; \beta)$ is defined in [6] and [7] by

$$\text{RSDPW}_m(\mathbf{s}_1\mathbf{s}_2; \boldsymbol{\beta}) = \max\{m(\mathbf{s}_1, \boldsymbol{\beta})/m(\mathbf{s}_2, \boldsymbol{\beta}), m(\mathbf{s}_2, \boldsymbol{\beta})/m(\mathbf{s}_1, \boldsymbol{\beta})\} \quad (13)$$

which measures the discriminatory power of the measure m by finding the maximum of two ratios, ratio of $m(\mathbf{s}_1, \boldsymbol{\beta})$ to $m(\mathbf{s}_2, \boldsymbol{\beta})$ and ratio of $m(\mathbf{s}_2, \boldsymbol{\beta})$ to $m(\mathbf{s}_1, \boldsymbol{\beta})$. The $\text{RSDPW}_m(\mathbf{s}_1, \mathbf{s}_2; \boldsymbol{\beta})$ defined by (13) provides a quantitative index of spectral discrimination capability of a specific hyperspectral measure m between the two spectral signatures $\mathbf{s}_1$ and $\mathbf{s}_2$ with respect to a third signature $\boldsymbol{\beta}$. Therefore, the higher the $\text{RSDPW}_m(\mathbf{s}_1, \mathbf{s}_2; \boldsymbol{\beta})$, the better the discriminatory power of m. In addition, $\text{RSDPW}_m(\mathbf{s}_1, \mathbf{s}_2; \boldsymbol{\beta})$ is symmetric and bounded below by one which is achieved by equality if and only if $\mathbf{s}_1 = \mathbf{s}_2$. It should be noted that the reference signature $\mathbf{r}$ used in the OSP-BPC for VNVBS is similar to the concept of using the third signature $\boldsymbol{\beta}$ in the RSDPW.

Using (13), Table IV tabulates the RSDPW obtained by full bands and the VNVBS using the SAM and the SID as the measures m in (13) with the signature $\boldsymbol{\beta}$ chosen to be the reference signature $\mathbf{r}$ which is the averaged signature over blackbrush, creosote leave, and sagebrush, denoted by $(\text{blackbrush} + \text{creosote leaves} + \text{sagebrush})/3$.

The experimental results in Table IV demonstrated that the relative discriminatory powers were significantly increased by using the VNVBS in the sense that the higher their RSDPW, the better the discrimination between the two signatures. On the other hand, the smaller their RSDPW, the more difficult the discrimination between the two signatures.

In order to have a better visual assessment, Figs. 4 and 5 also show the graphical representations of Table IV, where the RSDPW was graphically plotted as y-axis against a pair of signatures $(\mathbf{s}_1, \mathbf{s}_2)$ along the x-axis with $\boldsymbol{\beta}$ specified by the reference signature $\mathbf{r}$. For example, $1{:}(\mathbf{b}, \mathbf{c})$ in Fig. 4 represents $\text{RSDPW}_{\text{SAM}}(\mathbf{s}_1, \mathbf{s}_2; \boldsymbol{\beta})$ of the SAM comparing $\mathbf{s}_1 =$ '$\mathbf{blackbrush}$' against $\mathbf{s}_2 =$ '$\mathbf{creosote\ leaves}$' with $\boldsymbol{\beta} = \mathbf{r} = (\text{blackbrush} + \text{creosote leaves} + \text{sagebrush})/3$.

Based on Figs. 4 and 5, a tremendous improvement of the RSDPW that is produced by VNVBS over the full bands was visually apparent because the RSDPW between the blackbrush $(\mathbf{b})$ and the sagebrush $(\mathbf{s})$ was reduced, and the other two pairs

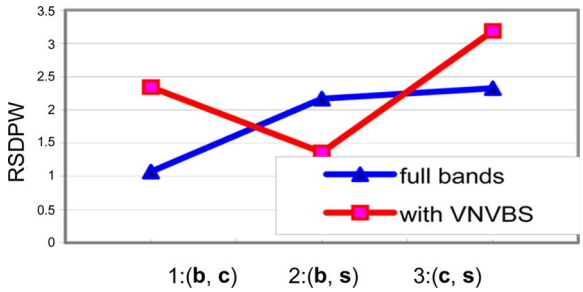

Fig. 4. Comparison between RSDPW of VNVBS and full bands using SAM.

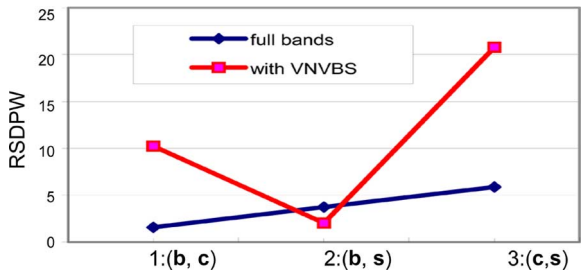

Fig. 5. Comparison between RSDPW of VNVBS and full bands using SID.

TABLE V
$\Omega_{\mathbf{s}}^{\perp}$ AND $\Omega_{\mathbf{s}}$ FOR BLACKBRUSH, CREOSOTE LEAVES, AND SAGEBRUSH

	$\Omega_{\mathbf{s}}^{\perp}$	$\Omega_{\mathbf{s}}$
Blackbrush	25,26	1-24, 27-158
Creosote leaves	47,48,49	1-46, 50-158
Sagebrush	43-48	1-42, 49-158
Drygrass	13-23, 92-98, 119-158	1-12, 24-91, 99-118,
$\mathbf{t}^{\text{mix}}$	none	1-158

$(\mathbf{b}, \mathbf{c})$ and $(\mathbf{c}, \mathbf{s})$ were greatly increased. More specifically, the contrast between similarity and dissimilarity of two signatures in terms of the RSDPW has been significantly enhanced and increased by using the VNVBS. Furthermore, comparing Fig. 4 to Fig. 5, the SID was also shown to outperform the SAM in the discrimination between the blackbrush, the creosote leave, and the sagebrush because the RSDPW of the SID was much higher than that of the SAM in terms of the contrast between the signature similarity and the signature dissimilarity. Because of that, only the SID would be used for study and analysis in the following experiments.

2) Signature Classification/Identification: In this section, we further assume that there is a class of signatures, blackbrush $(\mathbf{b})$, creosote leaves $(\mathbf{c})$, dry grass $(\mathbf{d})$, and sagebrush $(\mathbf{s})$, of interest for classification. We then simulated a mixed signature $\mathbf{t}^{\text{mix}}$ by uniformly mixing 1/4 $\mathbf{b}$, 1/4 $\mathbf{c}$, 1/4 $\mathbf{d}$, and 1/4 $\mathbf{s}$ as follows:

$$\mathbf{t}^{\text{mix}} = 0.25 \cdot \mathbf{b} + 0.25 \cdot \mathbf{c} + 0.25 \cdot \mathbf{d} + 0.25 \cdot \mathbf{s}. \qquad (14)$$

According to the results in [6] and [7], the spectral signature of the blackbrush is more close to the signature of sagebrush than to the signature of creosote leaves. Similarly, the spectral signature of the creosote leaves is more close to the signature of sagebrush than to the signature of blackbrush. Therefore, both blackbrush and creosote leaves can be considered as mutated signatures of the sagebrush. In this case, the total amount of abundance fractions that is contributed by blackbrush, creosote leaves, and sagebrush was 75% compared to only 25%

TABLE VI
SID, RESCALED SID, AND RSDPW BETWEEN $\mathbf{t}^{\text{mix}}$ AND EACH COMPONENT USING THE BANDS OBTAINED BY (12) AND TABLE V

full bands / VNVBS	$(\mathbf{t}^{\text{mix}},\mathbf{b})$	$(\mathbf{t}^{\text{mix}},\mathbf{s})$	$(\mathbf{t}^{\text{mix}},\mathbf{c})$	$(\mathbf{t}^{\text{mix}},\mathbf{d})$
SID	0.0052 / 5e-005	0.0081 / 1e-006	0.0661 / 2e-005	0.0500 / 0.0039
Rescaled SID	1 / 50	1.56 / 1	12.71 / 20	9.62 / 3900
RSDPW	192.2 / 20096	123.3 / 935720	15.123 / 45974	20.00 / 254.71

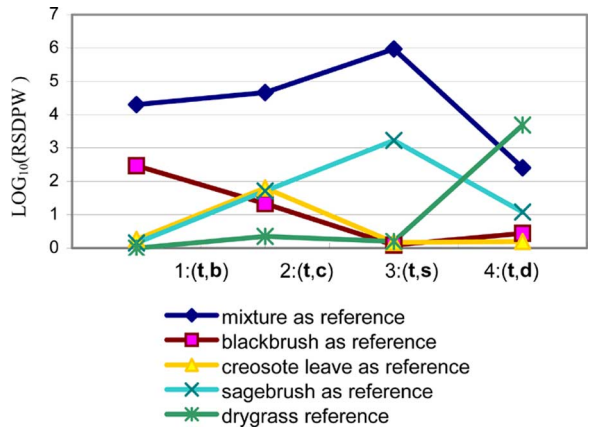

Fig. 6. RSDPW curves corresponding to the five different selections of reference signatures in using the VNVBS with a similarity measured by SID.

TABLE VII
SID VALUES BETWEEN $\tilde{\mathbf{t}}^{\text{mix}}$ AND EACH OF ITS COMPONENTS $\mathbf{b}$, $\mathbf{c}$, $\mathbf{d}$, AND $\mathbf{s}$ WITH THREE SNRS 10, 20, AND 30 dB

full / VNVBS	$(\tilde{\mathbf{t}}^{\text{mix}},\mathbf{b})$	$(\tilde{\mathbf{t}}^{\text{mix}},\mathbf{c})$	$(\tilde{\mathbf{t}}^{\text{mix}},\mathbf{s})$	$(\tilde{\mathbf{t}}^{\text{mix}},\mathbf{d})$
10dB	0.0074 / 0.0052	0.0674 / 0.0062	0.0100 / 0.0068	0.0532 / 0.0073
20dB	0.0052 / 0.0125	0.0662 / 0.0351	0.0081 / 0.0029	0.0500 / 0.0058
30dB	0.0052 / 0.00005	0.0661 / 0.00002	0.0081 / 0	0.0500 / 0.0039

TABLE VIII
RSDPW VALUES BETWEEN $\tilde{\mathbf{t}}^{\text{mix}}$ AND EACH OF ITS COMPONENTS $\mathbf{b}$, $\mathbf{c}$, $\mathbf{d}$, AND $\mathbf{s}$ WITH THREE SNRS 10, 20, AND 30 dB

full / VNVBS	$(\tilde{\mathbf{t}}^{\text{mix}},\mathbf{b})$	$(\tilde{\mathbf{t}}^{\text{mix}},\mathbf{c})$	$(\tilde{\mathbf{t}}^{\text{mix}},\mathbf{s})$	$(\tilde{\mathbf{t}}^{\text{mix}},\mathbf{d})$
10dB	137.41 / 14.62	15.05 / 4.82	107.52 / 11.28	18.55 / 8.34
20dB	194.71 / 12.03	15.13 / 4.78	123.59 / 17.96	19.94 / 10.00
30dB	192.30 / 12.12	15.12 / 4.77	123.37 / 18.05	19.99 / 10.04

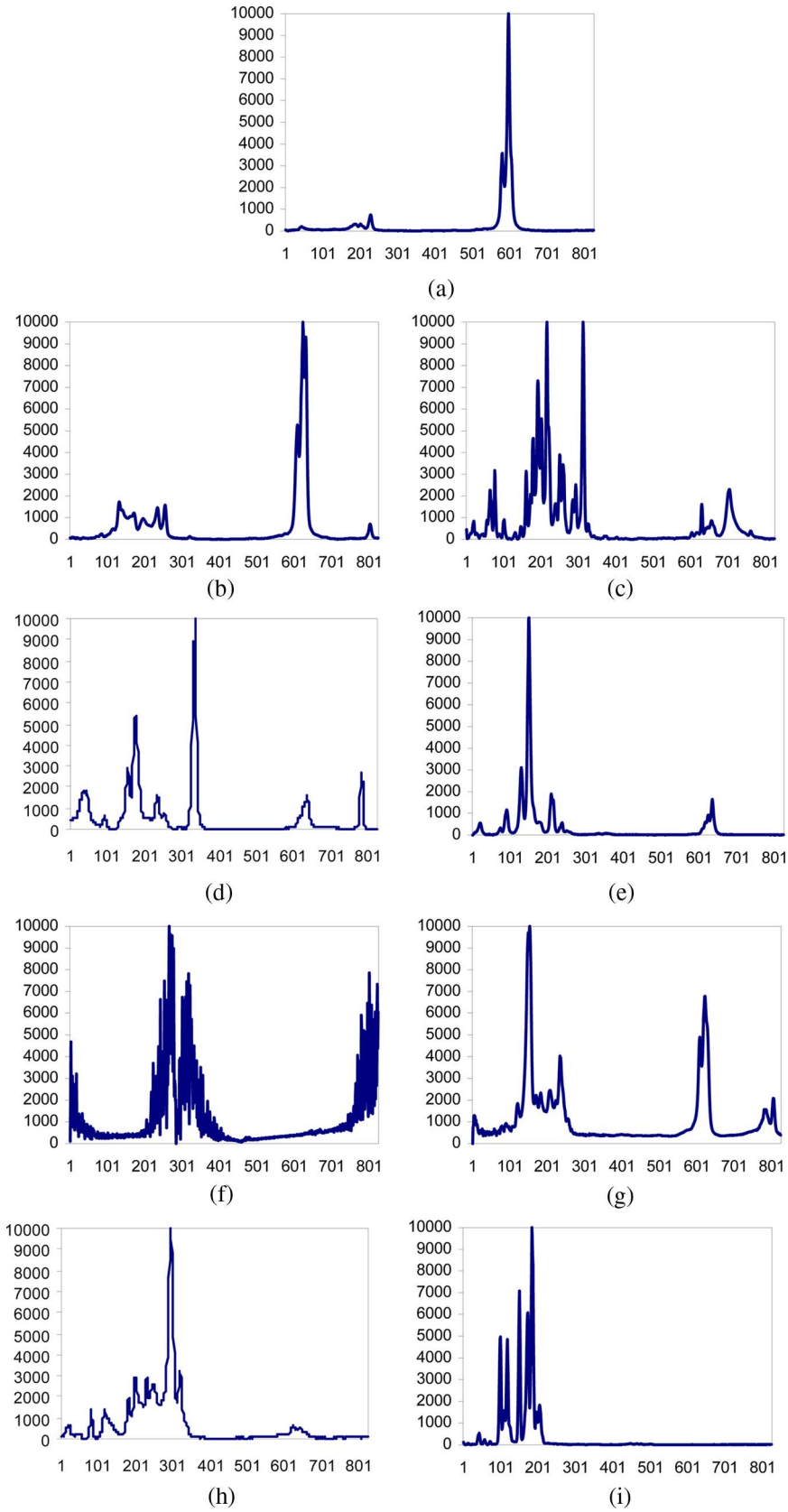

Fig. 7. Reflectances of the nine agent signatures from the data set Δ. (a) $\mathbf{s}_1$. (b) $\mathbf{s}_2$. (c) $\mathbf{s}_3$. (d) $\mathbf{s}_4$. (e) $\mathbf{s}_5$. (f) $\mathbf{s}_6$. (g) $\mathbf{s}_7$. (h) $\mathbf{s}_8$. (i) $\mathbf{s}_9$.

contributed by drygrass. As a result, it is natural to conclude that the mixture signature $\mathbf{t}^{\mathrm{mix}}$ in (14) should be classified as sagebrush because the sagebrush contributes more to the mixed pixel than any other three signatures. This interesting scenario sheds some light on the impact of BS on signature analysis. In this case, the reference signature $\mathbf{r}$ for VNVBS is simply chosen

to be the $\mathbf{t}^{\mathrm{mix}}$; Table V lists the bands prioritized by the VNVBS based on (9), where the original set of bands was divided into two subsets of bands $\Omega_{\mathbf{s}}^{\perp}$ and $\Omega_{\mathbf{s}}$ via (10).

Like Table I, $\Omega_{\mathbf{s}}^{\perp}$ was empty for $\mathbf{t}^{\mathrm{mix}}$. This is very obvious because the reference signature $\mathbf{r}$ specified by (3) and (4) is equal to the signature $\mathbf{s}$, both of which are $\mathbf{t}^{\mathrm{mix}}$. Table VI tabulates the spectral-similarity values measured by the SID between the VNVBS-generated new signatures of $\mathbf{t}^{\mathrm{mix}}$ and each of its components $\mathbf{b}$, $\mathbf{c}$, $\mathbf{d}$, and $\mathbf{s}$ according to the bands selected by Table V, where the upper and lower values in Table VI were obtained using the full band set and the priority-ranked band set $\Omega_{\mathbf{s}}^{\perp}$, respectively. In particular, the smallest SID value across a row is shaded for classification. The rescaled SID values, as well as the corresponding RSDPW values with $\boldsymbol{\beta}$ specified by $\mathbf{t}^{\mathrm{mix}}$, are also shown in Table VI for direct comparisons.

The results in Table VI demonstrated that the SID, using the VNVBS, greatly improved the performance for the mixed signature classification over the SID using full bands because the former could correctly classify the mixed signature into sagebrush while the latter could not. In addition, the contrast between different discrimination powers provided by the SID was also increased by using the VNVBS compared to that by using the full bands as shown by the rescaled SID in the second row of Table VI. For example, the maximum ratio between these two pairs using full bands is only 12.71 as opposed to 3900 using the VNVBS.

In order to further investigate the impact of the reference signature used by the VNVBS, experiments with different choices of reference signatures $\mathbf{r}$ were conducted where five choices were made for the reference signature $\mathbf{r}$, which are $\mathbf{t}^{\mathrm{mix}}$, blackbrush, creosote leaves, sagebrush, and drygrass, respectively. As a result, five $\mathrm{RSDPW}_{\mathrm{SID}}(\mathbf{t}, \mathbf{x}; \boldsymbol{\beta})$ plots were generated, each of which is produced by one particular choice of reference signature $\mathbf{r}$, as shown in Fig. 6, with the SID used as a spectral similarity measure, where "$\mathbf{t}$" is $\mathbf{t}^{\mathrm{mix}}$, and "$\mathbf{x}$" can be any one of the four signatures "$\mathbf{b}$," "$\mathbf{c}$," "$\mathbf{s}$," and "$\mathbf{d}$," which represent blackbrush, creosote leaves, sagebrush, and drygrass, respectively, with $\boldsymbol{\beta} = \mathbf{t}^{\mathrm{mix}}$. In addition, the interpretation of the RSDPW between the two signatures in Fig. 6 is the same as that made in Figs. 4 and 5.

As shown in Fig. 6, using $\mathbf{t}^{\mathrm{mix}}$ as the reference signature seemed to outperform any other selected reference signature.

The aforementioned experiments can also be used for the mixed signature identification if a class of signatures to be classified is replaced by a database or spectral library. In this case, the mixed signature $\mathbf{t}^{\mathrm{mix}}$ would be identified as the sagebrush via the assumed database $\Delta = \{\mathbf{b}, \mathbf{c}, \mathbf{d}, \mathbf{s}\}$.

3) Noise Effect on Performance of VNVBS: Finally, this section concludes with an investigation of noise effects on the performance of the VNVBS.

Adding a Gaussian noise $\mathbf{n}$ to (14) yields a noisy mixed signature as follows:

$$\widetilde{\mathbf{t}}^{\mathrm{mix}} = 0.25 \cdot \mathbf{b} + 0.25 \cdot \mathbf{c} + 0.25 \cdot \mathbf{d} + 0.25 \cdot \mathbf{s} + \mathbf{n}. \quad (15)$$

Since it was shown in Section IV-A2 that $\mathbf{t}^{\mathrm{mix}}$ was a better option for the reference signature, $\widetilde{\mathbf{t}}^{\mathrm{mix}}$ was also selected as the reference signature $\mathbf{r}$. Table VII tabulates the SID-measured spectral-similarity values between $\widetilde{\mathbf{t}}^{\mathrm{mix}}$ and each component $\mathbf{b}$, $\mathbf{c}$, $\mathbf{d}$, and $\mathbf{s}$, respectively, where a Gaussian noise was used to produce three different SNRs 10, 20, and 30 dB, as defined in [8]. The upper and lower rows in Table VII are the SID values obtained by using the VNVBS and the full bands, respectively, where the smallest SID value is shaded to indicate the classification of $\widetilde{\mathbf{t}}^{\mathrm{mix}}$.

As a comparison, the RSDPW values between $\widetilde{\mathbf{t}}^{\mathrm{mix}}$ and each component with three SNRs are shown in Table VIII as well. Similarly, the upper and lower rows in Table VIII are the RSDPW values obtained by using the VNVBS and the full bands, respectively.

An interesting finding can be observed from Tables VII and VIII. The higher the SNR value, the lower the noise level relative to the signal and vice versa. Therefore, based on Tables VII and VIII, when SNR $= 10$ dB, which means that the noise level is high and the signal is overwhelmed by noise, the SID values obtained by both the VNVBS and the full bands classified the $\widetilde{\mathbf{t}}^{\mathrm{mix}}$ as blackbrush instead of sagebrush, as the noise-free case did in Table VI in Section IV-A2, since the spectral shape, particularly the local spectral profile, has experienced significant distortion due to the noise effects. However, when SNR $= 20$ dB or 30 dB, it implies that the signal begins to show its dominance compared to the case of SNR $= 10$ dB. As a result, the SID values using the VNVBS correctly classify $\widetilde{\mathbf{t}}^{\mathrm{mix}}$ as sagebrush compared to the SID values using full bands which still classified $\widetilde{\mathbf{t}}^{\mathrm{mix}}$ as blackbrush. This experiment further showed the advantage of using the VNVBS over using the full bands.

TABLE IX
$\Omega_{\mathbf{s}}^{\perp}$ AND $\Omega_{\mathbf{s}}$ FOR EIGHT AGENTS $\{\mathbf{s}_i\}_{i=2}^{9}$

agent	$\Omega_{\mathbf{s}}^{\perp}$	$\Omega_{\mathbf{s}}$
$\mathbf{s}_2$	599 - 636	1-598, 637 - 880
$\mathbf{s}_3$	61 – 69, 74 – 80, 190 – 196, 212 – 222, 309 – 317, 692 - 720	1 – 60, 70 – 73, 81 – 189, 197 – 211, ,223 – 308 318 – 691, 721 - 880
$\mathbf{s}_4$	28 – 51, 327 - 343	1 – 27, 52 – 326, 344 - 880
$\mathbf{s}_5$	127 - 132	1- 126, 133 - 880
$\mathbf{s}_6$	1 – 9, 12 – 17, 262 – 281 301 – 309, 318 – 324 344 – 398, 403 – 407 736 – 740, 742 - 880	10, 11, 18 – 261, 282 – 300 310 – 317, 325 – 343 399 – 402, 408 – 735, 741
$\mathbf{s}_7$	138 – 146, 154 – 159, 383, 389 – 538, 554 – 597 605 - 613	1-137, 147-153, 160-382 384 – 388, 539-553 598 – 604, 614 - 880
$\mathbf{s}_8$	282 - 305	1-281, 306 -880
$\mathbf{s}_9$	95 – 122, 182 - 189	1-94, 123 – 181, 190 - 880

B. CB Data

In this section, the data set Δ to be used for experiments was the same as that considered in [11] and is available at the National Institute of Standard Technology's website [12].

TABLE X
DISCRIMINATION AMONG THE EIGHT AGENT SIGNATURES USING (12) AND TABLE IX WITH SID AND RSDPW USED AS SIMILARITY MEASURES ON THE UPPER AND LOWER TRIANGLES

VNVBS / full bands	$\mathbf{s}_2$	$\mathbf{s}_3$	$\mathbf{s}_4$	$\mathbf{s}_5$	$\mathbf{s}_6$	$\mathbf{s}_7$	$\mathbf{s}_8$	$\mathbf{s}_9$
$\mathbf{s}_2$	0 0	5.490 3.648	6.053 3.514	1.499 2.202	6.021 4.480	0.002 1.069	6.975 3.645	9.157 6.100
$\mathbf{s}_3$	5.391 1.217	0 0	5.371 3.155	3.966 3.949	2.597 3.204	3.506 2.484	2.456 1.676	5.845 4.724
$\mathbf{s}_4$	4.522 1.054	1.192 1.154	0 0	6.223 2.943	4.354 3.934	3.721 2.185	6.062 3.383	7.420 4.523
$\mathbf{s}_5$	2.905 1.140	15.665 1.388	13.138 1.202	0 0	5.491 5.301	1.454 1.134	6.409 4.118	3.373 3.123
$\mathbf{s}_6$	14.843 1.404	2.752 1.153	3.282 1.331	43.121 1.601	0 0	2.338 2.396	0.127 2.495	7.804 7.019
$\mathbf{s}_7$	1.944 3.235	2.772 2.657	2.325 3.068	5.649 3.689	7.633 2.304	0 0	4.664 2.506	4.198 3.824
$\mathbf{s}_8$	5.544 1.469	1.028 1.206	1.226 1.393	16.108 1.675	2.677 1.046	2.851 2.201	0 0	7.423 5.350
$\mathbf{s}_9$	7.568 2.066	1.403 2.515	1.673 2.178	21.989 1.811	1.961 2.901	3.892 6.685	1.365 3.035	0 0

It contains nine agent signatures $\{\mathbf{s}_i\}_{i=1}^{9}$, eight of them $\{\mathbf{s}_i\}_{i=2}^{9}$ are composed of 880 bands, and only one of them $\mathbf{s}_1$ consists of 825 bands. Fig. 7 shows the signature waveforms of the nine agents in data set Δ.

1) Signature Discrimination for Agents $\mathbf{s}_2$–$\mathbf{s}_9$: In this section, the eight agent signatures $\{\mathbf{s}_i\}_{i=2}^{9}$, with the same number of bands, were used as signatures to be discriminated. The agent $\mathbf{s}_1$ was removed from consideration because it has a different number of bands from those used in other eight signatures. As a result, the reference signature $\mathbf{r}$ for the OSP-BPC was chosen to be the averaged signature over $\mathbf{s}_2$, $\mathbf{s}_3$, $\mathbf{s}_4$, $\mathbf{s}_5$, $\mathbf{s}_6$, $\mathbf{s}_7$, $\mathbf{s}_8$, and $\mathbf{s}_9$. Table IX lists the bands prioritized by the OSP-BPC based on (9), where the original set of bands Ω was divided into two subsets of bands $\Omega_{\mathbf{s}}^{\perp}$ and $\Omega_{\mathbf{s}}$ via (10).

Table X tabulates the spectral-similarity values of the SID that are produced by the VNVBS and the full bands in discriminating among the eight different agent signatures from $\mathbf{s}_2$ to $\mathbf{s}_9$, where the VNVBS was implemented via (12) and the bands were tabulated in Table IX. Since Table X is symmetric, the SID and RSDPW values are tabulated in the upper and lower triangles of Table X, respectively. As shown in Table X, the signature-discrimination performance was improved significantly by the VNVBS over that produced by using the full bands. In order to have a better visual assessment, Fig. 8 shows the graphical representation of Table X, where the RSDPW was graphically plotted as y-axis against the pairs of signatures along the x-axis on the order of $(\mathbf{s}_2, \mathbf{s}_3), (\mathbf{s}_2, \mathbf{s}_4), \ldots, (\mathbf{s}_2, \mathbf{s}_9)$, $(\mathbf{s}_3, \mathbf{s}_4), \ldots, (\mathbf{s}_3, \mathbf{s}_9), \ldots, (\mathbf{s}_8, \mathbf{s}_9)$ with $\boldsymbol{\beta}$ specified by the reference signature $\mathbf{r}$. For example, $(\mathbf{s}_j, \mathbf{s}_k)$ in Fig. 8 represents $\mathrm{RSDPW}_{\mathrm{SID}}(\mathbf{s}_j, \mathbf{s}_k; \boldsymbol{\beta})$ of the SID comparing $\mathbf{s}_j$ against $\mathbf{s}_k$ with the $\boldsymbol{\beta}$ set to the reference signature $\mathbf{r}$, which was the averaged signature over $\mathbf{s}_2$ to $\mathbf{s}_9$. As shown in Fig. 8, the SID using VNVBS clearly outperformed the SID using full bands.

2) Signature Classification/Identification Agents $\mathbf{s}_2$–$\mathbf{s}_9$: Following the same arguments made in Section IV-A2, we also simulated a mixed signature $\mathbf{t}^{\mathrm{mix}}$ by uniformly mixing eight different agent signatures from $\mathbf{s}_2$ to $\mathbf{s}_9$, namely,

$$\mathbf{t}^{\mathrm{mix}} = 0.125 \cdot \mathbf{s}_2 + 0.125 \cdot \mathbf{s}_3 + 0.125 \cdot \mathbf{s}_4 + 0.125 \cdot \mathbf{s}_5 + 0.125 \cdot \mathbf{s}_6 + 0.125 \cdot \mathbf{s}_7 + 0.125 \cdot \mathbf{s}_8 + 0.125 \cdot \mathbf{s}_9 \quad (16)$$

with the reference signature $\mathbf{r}$, which was chosen to be the same as that used in Section IV-B1. As a result, in this particular case, the reference signature $\mathbf{r}$ turns out to be the same signature to be classified $\mathbf{t}^{\mathrm{mix}}$. Table XI tabulates the spectral-similarity values that are produced by the SID between $\mathbf{t}^{\mathrm{mix}}$ and each of the eight agents $\{\mathbf{s}_i\}_{i=2}^{9}$ using the full bands and the VNVBS, where the upper and lower values in each entry of Table XI were obtained by the VNVBS and all the full 880 bands, respectively, and the smallest value is shaded for classification.

Like the AVIRIS experiments, the signature-discrimination performance was significantly improved by using the VNVBS compared to that produced by using the full bands. Fig. 9 also shows the graphical representation of the RSDPW obtained from Table XI, where the RSDPW was graphically plotted

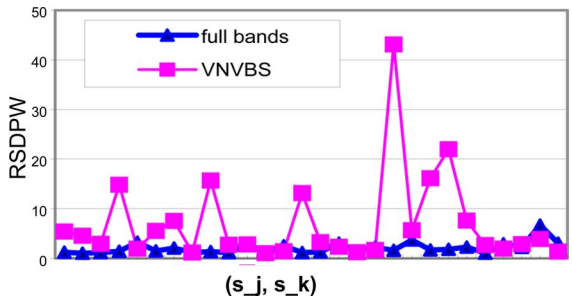

Fig. 8. Comparison between RSDPW of VNVBS and full bands using the SID for signature discrimination among eight agents.

TABLE XI
SID, RESCALED SID, AND RSDPW BETWEEN MIXED SIGNATURE AND EACH COMPONENT WITH AND WITHOUT VNVBS USING THE BANDS OBTAINED BY (12)

VNVBS / full bands	$(\mathbf{t}^{mix}, \mathbf{s}_2)$	$(\mathbf{t}^{mix}, \mathbf{s}_3)$	$(\mathbf{t}^{mix}, \mathbf{s}_4)$	$(\mathbf{t}^{mix}, \mathbf{s}_5)$	$(\mathbf{t}^{mix}, \mathbf{s}_6)$	$(\mathbf{t}^{mix}, \mathbf{s}_7)$	$(\mathbf{t}^{mix}, \mathbf{s}_8)$	$(\mathbf{t}^{mix}, \mathbf{s}_9)$
SID	2.17 / 1.68	0.007 / 1.38	1.84 / 1.60	2.73 / 1.92	0.003 / 1.20	0.001 / 0.52	2.37 / 1.15	3.93 / 3.48
Rescaled SID	2170 / 3.23	7 / 2.65	1840 / 3.08	2730 / 3.69	3 / 2.31	1 / 1	2370 / 2.21	3930 / 6.69
RSDPW	138.33 / 1.683	25.654 / 1.383	30.589 / 1.597	401.87 / 1.920	9.319 / 1.199	71.137 / 1.992	24.949 / 1.146	16.276 / 3.479

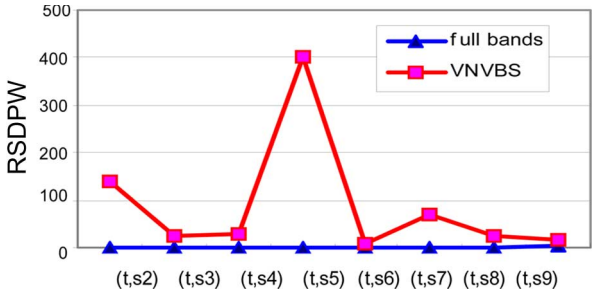

Fig. 9. Comparison between RSDPW of VNVBS and full bands using the SID for mixed signature classification.

as y-axis against the pairs of signatures $(\mathbf{t}^{\text{mix}}, \mathbf{s}_k)$ with $k = 2, 3, \ldots, 9$ along the x-axis with $\boldsymbol{\beta}$ specified by the reference signature $\mathbf{r}$. For example, $(\mathbf{t}, \mathbf{s}_j)$ in Fig. 9 represents the $\text{RSDPW}_{\text{SID}}(\mathbf{t}^{\text{mix}}, \mathbf{s}_j; \boldsymbol{\beta})$ produced by the SID comparing $\mathbf{t}^{\text{mix}}$ against $\mathbf{s}_j$ with the $\boldsymbol{\beta}$ set to the reference signature $\mathbf{r}$, which was the averaged signature over $\mathbf{s}_2$ to $\mathbf{s}_9$. Once again, as shown in Fig. 9, the VNVBS demonstrated its superior performance to that produced by using the full bands in terms of the rescaled values of SID, as shown in the second row of Table XI. For example, the maximum SID ratio using the full bands between eight pairs of $(\mathbf{t}^{\text{mix}}, \mathbf{s}_i)$ with $i = 2, 3, \ldots, 9$ is only 6.69 compared to 3930 using the VNVBS.

3) Signature Discrimination Between Two Signatures With Different Numbers of Bands: One of the strengths of the VNVBS is its ability to discriminate two signatures with different numbers of bands that was not found in the AVIRIS experiments. In order to demonstrate this advantage, the agent $\mathbf{s}_1$ with 825 bands was used for this purpose to be compared against the other eight agents $\mathbf{s}_2$–$\mathbf{s}_9$ with 880 bands. In doing so, two approaches are considered. One is to extract bands from the signature with a larger number of bands to match the same number of bands that are used by the signature with a smaller number of bands. As an opposite to the first approach, a second approach is to expand the signature with a smaller number of bands to match the same number of bands that are used by the signature with a larger number of bands by zero-padding in the missing bands. These two approaches are considered in the following experiments.

Approach 1—Extracting 825 bands from the original 880 bands for $\mathbf{s}_2$–$\mathbf{s}_9$ with the same wavelength coverage as $\mathbf{s}_1$: In this case, the reference signature $\mathbf{r}$ for the VNVBS was chosen by averaging from $\mathbf{s}_1$ to $\mathbf{s}_9^*$, where $\mathbf{s}_j^*(j = 2, 3, \ldots, 9)$ denotes the signature with 825 bands extracted from the jth signature with the original 880 bands. In this case, the $\mathbf{r}$ has only 825 bands.

TABLE XII
$\Omega_{\mathbf{s}}^{\perp}$ AND $\Omega_{\mathbf{s}}$ GENERATED BY APPROACH 1 FROM $\mathbf{s}_1$ TO $\mathbf{s}_9$

$\mathbf{s}$	$\Omega_{\mathbf{s}}^{\perp}$	$\Omega_{\mathbf{s}}$
$\mathbf{s}_1$	596	1-595, 597-825
$\mathbf{s}^*_2$	581-611	1-580, 612-825
$\mathbf{s}^*_3$	37-44, 49-55, 165-171, 187-197, 284-292, 667-695	1-36, 45-48, 56-164, 172-186, 198-283, 293-666, 696-825
$\mathbf{s}^*_4$	2-26, 302-318	1, 27-301, 319-825
$\mathbf{s}^*_5$	102-107	1-101, 108-825
$\mathbf{s}^*_6$	237-256, 275-284, 293,300, 319-382, 705, 710-825	1-236, 257-274, 285-292, 294-299, 301-318, 383-704, 706-709
$\mathbf{s}^*_7$	113-121, 129-134, 358, 364-366, 368-506	1-112, 122-128, 135-357, 359-363, 367, 507-825
$\mathbf{s}^*_8$	257-280	1-256, 281-825
$\mathbf{s}^*_9$	70-79, 82-86, 89-97, 157-164	1-69, 80-81, 87-88, 98-156, 165-825

Table XII lists the bands that are prioritized by the VNVBS based on (9), where the original set of bands was divided into two subsets of bands $\Omega_{\mathbf{s}}^{\perp}$ and $\Omega_{\mathbf{s}}$ via (10).

Table XIII tabulates the SID-generated spectral-similarity values that are obtained by the VNVBS and the full bands, respectively, for comparison, where the VNVBS also outperformed the use of full bands. Similar to Table X, the SID and RSDPW values are tabulated in the upper and lower triangles of Table XIII, respectively.

Approach 2—Expanding the original 825 bands to 880 bands through zero-padding: In this case, $\mathbf{s}_1^{\wedge}$ denotes the signature $\mathbf{s}_1$ after interpolating the original 825 bands to 880 bands by zero-padding. Similarly, Table XIV lists the bands that are prioritized by the VNVBS based on (9), where the original set of bands was divided into two subsets of bands $\Omega_{\mathbf{s}}^{\perp}$ and $\Omega_{\mathbf{s}}$ via (10).

Table XV tabulates the SID-generated spectral-similarity values with the VNVBS and the full bands, respectively, for comparison. Like Table XIII, the SID and RSDPW values are tabulated in the upper and lower triangles of Table XV, respectively, where the VNVBS also demonstrated its advantage by selecting bands compared to the full bands.

TABLE XIII
DISCRIMINATION AMONG THE NINE AGENT SIGNATURES FROM $\mathbf{s}_1$ TO $\mathbf{s}_9^*$ OBTAINED BY VNVBS AND FULL BANDS

VNVBS / full bands	$\mathbf{s}_1$	$\mathbf{s}_2^*$	$\mathbf{s}_3^*$	$\mathbf{s}_4^*$	$\mathbf{s}_5^*$	$\mathbf{s}_6^*$	$\mathbf{s}_7^*$	$\mathbf{s}_8^*$	$\mathbf{s}_9^*$
$\mathbf{s}_1$	0 0	0.18 0.63	5.08 4.80	7.77 4.95	6.34 4.24	6.01 5.51	3.27 2.17	8.11 4.82	9.74 8.96
$\mathbf{s}_2^*$	1.01 1.72	0 0	5.29 3.62	6.14 3.51	1.67 2.17	5.94 4.40	1.38 1.04	7.26 3.67	8.94 6.08
$\mathbf{s}_3^*$	4.10 1.79	4.14 1.04	0 0	5.36 3.17	3.96 4.00	259 2.97	3.31 2.48	2.45 1.70	5.84 4.73
$\mathbf{s}_4^*$	3.61 1.62	3.65 1.05	1.13 1.10	0 0	6.15 2.99	4.00 3.56	3.52 2.15	6.04 3.43	7.41 4.48
$\mathbf{s}_5^*$	3.84 1.33	3.79 1.28	15.75 1.34	13.87 1.21	0 0	5.72 5.25	1.19 1.30	6.40 4.20	3.37 3.06
$\mathbf{s}_6^*$	10.93 1.99	11.05 1.16	2.66 1.11	3.02 1.22	42.00 1.49	0 0	2.23 2.36	0.18 2.16	7.80 6.75
$\mathbf{s}_7^*$	1.23 5.30	1.24 3.08	3..33 2.95	2.93 3.26	4.72 3.96	8.88 2.65	0 0	4.99 2.54	3.06 3.74
$\mathbf{s}_8^*$	4.17 2.12	4.22 1.23	1.01 1.18	1.15 1.30	16.04 1.59	2.61 1.06	3.39 2.49	0 0	7.42 5.36
$\mathbf{s}_9^*$	5.73 1.41	5.79 2.43	1.39 2.53	1.58 2.30	22.02 1.89	1.90 2.82	4.65 7.50	3.37 3.01	0 0

TABLE XIV
$\Omega_{\mathbf{s}}^{\perp}$ AND $\Omega_{\mathbf{s}}$ GENERATED BY APPROACH 2 FROM $\mathbf{s}_1$ to $\mathbf{s}_9$

$\mathbf{s}$	$\Omega_{\mathbf{s}}^{\perp}$	$\Omega_{\mathbf{s}}$
$\hat{\mathbf{s}}_1$	1-23, 620-621, 853-880	24-619, 622-852
$\mathbf{s}_2$	606-613, 624-636	1-605, 614-623, 637-880
$\mathbf{s}_3$	61-69, 74-80, 190-196, 212-222, 309-317, 692-720	1-60, 70-73, 81-189, 197-211, 223-308, 318-691, 721-880
$\mathbf{s}_4$	28-51, 327-343	1-27, 52-326, 344-880
$\mathbf{s}_5$	127-132	1-126, 133-880
$\mathbf{s}_6$	1-18, 262-281, 301-309, 318-325, 344-399, 403-407, 735-880	19-261, 282-300, 310-317, 326-343, 400-402, 408-734
$\mathbf{s}_7$	138-146, 154-159, 383, 389-531	1-137, 147-153, 160-382, 384-388, 532-880
$\mathbf{s}_8$	282-305	1-281, 306-880
$\mathbf{s}_9$	95-122, 182-189	1-94, 123-181, 190-880

Based on Tables XIII and V, the two approaches did not have very much impact on the SID when full bands were used, but their discriminatory powers calculated for the rescaled SID and RSDPW values were significantly improved when the VNVBS was used for the SID.

One final comment is noteworthy. The two approaches proposed for the VNVBS in Section IV-B3 are specifically designed for signatures, not images, and are not applicable to the standard BS techniques [1]–[4] because we cannot process a hyperspectral image whose image pixels vary with different number of bands. The OSP-BPC proposed in this paper allows the users to implement the VNVBS for spectral characterization. To the authors' best knowledge, there are no existing standard BS techniques that can be used to select bands from a single hyperspectral signature, as what the VNVBS does. Such benefit derived from the VNVBS cannot be gained by any image-based BS [1]–[4].

By concluding this section, it is worth noting that there are significant differences between the two data sets, which are the CB data and the AVIRIS data. Of course, the VNVBS performed quite differently. The $\Omega_{\mathbf{s}}^{\perp}$ obtained for the CB data tended to capture the peaks, while the $\Omega_{\mathbf{s}}^{\perp}$ obtained for the hyperspectral AVIRIS data attempted to capture the edges of the spectral signatures. This is because the peaks in the CB data and edges in the AVIRIS data are their most distinct spectral features in their local spectral profiles. The VNVBS is particularly designed to characterize the local properties of a signature.

V. SELECTION OF REFERENCE SIGNATURES

As noted, the selection of the reference signature $\mathbf{r}$ has a significant impact on the performance. In order to address this issue, two general guidelines of how to select the reference signature $\mathbf{r}$ based on our extensive experiments may be helpful.

1) Since the signature $\mathbf{r}$ is used as a reference signature between the two signatures $\mathbf{s}_1$ and $\mathbf{s}_2$, it should have some degree of correlation associated with both signatures. Keeping this in mind, when the spectral feature characterization is performed, such as signature discrimination via a database/spectral library, the best reference signature to be selected is the average of all signatures in the database/spectral library so that any pair of the two signatures drawn from the database/spectral library to be characterized can have some correlation with the

TABLE XV
DISCRIMINATION AMONG THE NINE AGENT SIGNATURES FROM $\hat{\mathbf{s}}_1$ TO $\mathbf{s}_9$ OBTAINED BY VNVBS AND FULL BANDS

VNVBS / full bands	$\hat{\mathbf{s}}_1$	$\mathbf{s}_2$	$\mathbf{s}_3$	$\mathbf{s}_4$	$\mathbf{s}_5$	$\mathbf{s}_6$	$\mathbf{s}_7$	$\mathbf{s}_8$	$\mathbf{s}_9$
$\hat{\mathbf{s}}_1$	0 0	0.20 0.62	5.85 4.77	7.72 4.86	5.38 4.17	∞ 5.20	3.20 2.13	8.03 4.77	10.5 8.95
$\mathbf{s}_2$	130.96 1.65	0 0	5.29 3.64	6.15 3.50	1.67 2.19	5.86 4.47	1.38 1.05	7.26 3.64	8.94 6.05
$\mathbf{s}_3$	31.57 1.72	4.14 1.04	0 0	5.37 3.14	3.96 3.93	2.59 3.12	3.31 2.45	2.45 1.67	5.84 4.71
$\mathbf{s}_4$	37.21 1.52	3.51 1.07	1.17 1.13	0 0	6.22 2.91	4.30 3.81	3.54 2.14	6.06 3.37	7.41 4.49
$\mathbf{s}_5$	497.44 1.29	3.79 1.27	15.75 1.33	13.36 1.18	0 0	5.41 5.29	1.19 1.31	6.40 4.11	3.37 3.10
$\mathbf{s}_6$	11.63 1.94	11.25 1.17	2.71 1.12	3.19 1.27	42.74 1.50	0 0	2.17 2.38	0.12 2.29	7.79 6.81
$\mathbf{s}_7$	105.25 5.19	124 3.14	3.33 3.00	2.82 3.39	4.73 4.01	9.04 2.66	0 0	4.99 2.49	3.06 3.74
$\mathbf{s}_8$	31.00 2.07	4.22 1.25	1.01 1.20	1.20 1.35	16.04 1.60	2.66 1.06	3.39 2.49	0 0	7.42 5.33
$\mathbf{s}_9$	22.58 1.45	5.79 2.40	1.39 2.52	1.64 2.22	22.02 1.88	1.94 2.83	4.65 7.56	3.37 3.03	0 0

averaged signature. On the other hand, if a reference signature is selected from the database/spectral library, the performance will be determined by how close a signature is related to the other signature coming from the same database, which is to be compared against. As a consequence, the performance may yield complete different results. Such evidence was demonstrated in Section IV.

2) By contrast, if a mixed signature is to be classified/identified through a database/spectral library which is composed of each mixing component, then the best candidate for the reference signature $\mathbf{r}$ is the mixed signature itself. This is because the mixed signature itself already provides the desired correlation for the classification/identification between this mixed signature and each of its mixing components. Using the average of signatures may only smear the spectral characteristics. This was also confirmed by the experiments in Section IV-A2.

VI. CONCLUSION

This paper presents a new approach to BS for a single hyperspectral signature, which is called VNVBS. Unlike most BS techniques, which are designed for images, the proposed VNVBS is designed for the characterization of a single hyperspectral signature without a need of an image sample correlation. In order to select the appropriate bands, an OSP-BPC is also developed, which decomposes the original spectral signature into two orthogonal components that can be used for spectral characterization. The experimental results demonstrate that the proposed VNVBS is more effective in preserving information for the hyperspectral-signature characterization than that using the full-band information in the hyperspectral-signature characterization and analysis.

ACKNOWLEDGMENT

The authors would like to thank the anonymous reviewers for their comments which significantly improve the presentation and quality of this paper.

REFERENCES

[1] P. W. Mausel, W. J. Kramber, and J. K. Lee, "Optimum band selection for supervised classification of multispectral data," *Photogramm. Eng. Remote Sens.*, vol. 56, no. 1, pp. 55–60, Jan. 1990.
[2] C. Conese and F. Maselli, "Selection of optimum bands from TM scenes through mutual information analysis," *ISPRS J. Photogramm. Remote Sens.*, vol. 48, no. 3, pp. 2–11, 1993.
[3] S. D. Stearns, B. E. Wilson, and J. R. Peterson, "Dimensionality reduction by optimal band selection for pixel classification of hyperspectral imagery," in *Proc. SPIE, Appl. Digital Image Process. XVI*, 1993, vol. 2028, pp. 118–127.
[4] C.-I Chang, Q. Du, T. S. Sun, and M. L. G. Althouse, "A joint band prioritization and band decorrelation approach to band selection for hyperspectral image classification," *IEEE Trans. Geosci. Remote Sens.*, vol. 37, no. 6, pp. 2631–2641, Nov. 1999.
[5] R. Huang and M. He, "Band selection based feature weighting for classification of hyperspectral data," *IEEE Geosci. Remote Sens. Lett.*, vol. 2, no. 2, pp. 156–159, Apr. 2005.
[6] C.-I Chang, "An information theoretic-based approach to spectral variability, similarity and discriminability for hyperspectral image analysis," *IEEE Trans. Inf. Theory*, vol. 46, no. 5, pp. 1927–1932, Aug. 2000.
[7] C.-I Chang, *Hyperspectral Imaging: Techniques for Spectral Detection and Classification*. New York: Kluwer, 2003.
[8] J. C. Harsanyi and C.-I Chang, "Hyperspectral image classification and dimensionality reduction: An orthogonal subspace projection approach," *IEEE Trans. Geosci. Remote Sens.*, vol. 32, no. 4, pp. 779–785, Jul. 1994.
[9] R. C. Gonzalez and R. E. Woods, *Digital Image Processing*, 2nd ed. Englewood Cliffs, NJ: Prentice-Hall, 2001, p. 66.
[10] T. Cover and J. Thomas, *Elements of Information Theory*. Hoboken, NJ: Wiley, 1991.
[11] C. Kwan, B. Ayhan, G. Chen, J. Wang, B. Ji, and C.-I Chang, "A novel approach for spectral unmixing, classification, and concentration estimation of chemical and biological agents," *IEEE Trans. Geosci. Remote Sens.*, vol. 44, no. 2, pp. 409–419, Feb. 2006.
[12] [Online]. Available: webbook.nist.gov/chemistry

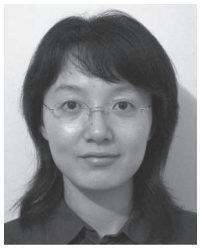

Su Wang (S'05–M'07) received the B.S. and M.S. degrees in electrical engineering from the Nanjing University of Aeronautics and Astronautics, Nanjing, China, in 2000 and 2003, respectively, and the Ph.D. degree in electrical engineering from the University of Maryland Baltimore County, Baltimore, in 2006.

With her priori achievements in signal and image processing, pattern recognition, and data compression in hyperspectral imagery, she is currently a Research Associate in the Health Science Center, Medical School, State University of New York, Stony Brook, working on computed-tomography image segmentation and computer-aided-diagnosis systems for the noninvasive early detection of colon cancer.

Chein-I Chang (S'81–M'87–SM'92) received the B.S. degree in mathematics from Soochow University, Taipei, Taiwan, R.O.C., the M.S. degree in mathematics from the Institute of Mathematics, National Tsing Hua University, Hsinchu, Taiwan, and the M.A. degree in mathematics from the State University of New York at Stony Brook, Stony Brook. He also received the M.S. and M.S.E.E. degrees from the University of Illinois at Urbana–Champaign, Urbana, and the Ph.D. degree in electrical engineering from the University of Maryland, College Park.

He has been at the University of Maryland Baltimore County, Baltimore, since 1987 and is currently a Professor in the Remote Sensing Signal and Image Processing Laboratory, Department of Computer Science and Electrical Engineering. He was a Visiting Research Specialist in the Institute of Information Engineering, National Cheng Kung University, Tainan, Taiwan, from 1994 to 1995. Additionally, he was a Distinguished Lecturer Chair at the National Chung Hsing University sponsored by the Department of Education and National Science Council, Taiwan, from 2005 to 2006 and is currently holding a Chair Professorship with the Environmental Restoration and Disaster Reduction Research Center and Department of Electrical Engineering, National Chung Hsing University, Taichung, Taiwan. He is the holder of three patents and has several pending patents on hyperspectral image processing. He is on the editorial board of the *Journal of High Speed Networks* and was the Guest Editor of a Special Issue of the same journal on Telemedicine and Applications and the Coguest Editor of two Special Issues on Broadband Multimedia Sensor Networks in Healthcare Applications, *Journal of High Speed Networks* (2007) and High Performance Computing of Hyperspectral Imaging, *International Journal of High Performance Computing Applications* (December 2007). He has authored the book *Hyperspectral Imaging: Techniques for Spectral Detection and Classification* (Kluwer Academic, 2003) and edited two books, *Recent Advances in Hyperspectral Signal and Image Processing* (Trivandrum, Kerala: Research Signpost, Trasworld Research Network, India, 2006) and *Hyperspectral Data Exploitation: Theory and Applications* (Wiley, 2007). He is currently working on his second book *Hyperspectral Imaging: Signal Processing Algorithm Design and Analysis* (Wiley, 2007) and coediting a book on *High Performance Computing in Remote Sensing* (CRC Press, 2007) with A. Plaza. His research interests include multispectral/hyperspectral image processing, automatic target recognition, medical imaging, information theory and coding, signal detection and estimation, and neural networks.

Dr. Chang was an Associate Editor in the area of hyperspectral signal processing for the IEEE TRANSACTIONS ON GEOSCIENCE AND REMOTE SENSING from 2001 to 2007, a Fellow of the International Society for Optical Engineering, and a member of Phi Kappa Phi and Eta Kappa Nu. He received the National Research Council Senior Research Associateship Award from 2002 to 2003, which was sponsored by the U.S. Army Soldier and Biological Chemical Command, Edgewood Chemical and Biological Center, Aberdeen Proving Ground, MD.